

TEMPERATURE EFFECT ON THE LOW-VELOCITY IMPACT
CHARACTERISTICS OF GLASS LAMINATED ALUMINIUM
REINFORCED EPOXY PANELS

CHOW ZHEN PEI

A thesis submitted in fulfilment of the
requirements for the award of the degree of
Doctor of Philosophy

School of Mechanical Engineering
Faculty of Engineering
Universiti Teknologi Malaysia

APRIL 2022

DEDICATION

This thesis is dedicated to my father, who taught me the importance of purpose and reasoning in the pursuit of knowledge, and to believe in myself. It is also dedicated to my mother, who taught me to have perseverance, determination and gave me endless support when I needed. To my brothers who gave me advices that helped me through difficult challenges. To my friends who provided encouragement and listened to my problems.

ACKNOWLEDGEMENT

First and foremost, I would like to express my sincere gratitude towards my main supervisor, Associate Prof. Ir. Ts. Dr. Zaini Ahmad for his expertise in guidance, giving advises and critics that helped me grow and improve. I am also very grateful towards my co-supervisor, Dr Wong King Jye for his patience and eagerness in helping and guiding me. Thanks to both my supervisors for contributing their precious time and efforts, for their motivation, support and understanding throughout my research work. Without their persistent supervision and support, I would not be able to complete my research and thesis.

I would like to thank Universiti Teknologi Malaysia (UTM) for the facilities, equipment and funds given that helped my research work. Thank the UTM staffs that provided their assistance during my experimental tests.

I am deeply appreciative towards my fellow colleagues in Computational Solid Mechanics (CSM) laboratory that aided and supported me. They provided me insightful advice for my research, assistance during experimental testing and improvement ideas for my simulation modelling. Regrettably, I am unable to mention all their names due to the limited space.

I would also like to extend my gratitude towards my friends, including Mahzan, Saied, Chiang, Salman, Izzuddin, Amirul and Syed that spend their time aiding me when I reached out to them and supported me when I require motivation.

ABSTRACT

Applications of fibre metal laminates (FML) in aircraft structures involve in-service temperatures higher than 30°C up to well above 100°C. Such high temperatures could affect the FML performance. Hence, there is a need to investigate temperature effect towards the low-velocity impact response of FMLs. The purpose of this study was to evaluate the influence of increased temperature from 30 to 110°C towards the impact response of FMLs. Experimental trials were conducted at 30, 70 and 110°C to extract temperature-dependent properties of glass fibre reinforced polymer (GFRP) composite and interlaminar delamination of GFRP laminated aluminium. The experimental results obtained from the quasi-static tests at 30, 70 and 110°C and low-velocity impact tests at various impact energies were used to validate the numerical models. Explicit nonlinear code LS-DYNA was subsequently employed to develop the finite element (FE) model of the FMLs. Johnson-Cook model, Chang-Chang failure criteria and cohesive zone models were applied to simulate aluminium, GFRP and delamination, respectively. The Mode-I and Mode-II delamination and quasi-static perforation of FMLs at elevated temperatures were modelled and validated. After which, combined analysis of impact energy levels and temperatures were carried out by employing the FE quarter model. A modified property degradation model was also utilised to obtain properties at 50 and 70°C effectively with a single fitting parameter. Using the validated FE model, parametric studies were carried out to investigate the effects of varying geometrical parameters at elevated temperature. The results indicated that an increase in temperature significantly affects the low-velocity impact response and impact resistance of FMLs. Increase in temperature degrades the GFRP and GFRP/aluminium interface by a larger degree as compared to aluminium. The degradation of FMLs is progressive such that it is less significant from 30 to 70°C and more severe from 70 to 110°C. Hence, the FE modelling methodology proposed herein provides the means to simulate, predict and analyse the impact of FMLs with consideration of temperature effects. This research contributes towards the advancement of FMLs and composites for applications under high temperatures. The FE method provides a coherent and reliable way to simulate and analyse FML impact performance under different temperature conditions.

ABSTRAK

Penggunaan lapisan logam gentian (FML) dalam struktur pesawat melibatkan suhu dalam perkhidmatan yang lebih tinggi daripada 30°C sehingga melebihi 100°C. Suhu yang tinggi boleh menjejaskan prestasi FML. Oleh itu, terdapat keperluan untuk menyelidik kesan suhu terhadap tindakan hentaman halaju rendah FML. Tujuan kajian ini adalah untuk menilai pengaruh peningkatan suhu dari 30 hingga 110°C terhadap tindakan hentaman FML. Ujikaji dijalankan pada suhu 30, 70 dan 110°C untuk ekstrak sifat bersandar suhu rencam polimer bertetulang gentian kaca (GFRP) dan pelekangan antara lapisan aluminium GFRP. Keputusan ujikaji yang diperolehi daripada ujian kuasi-statik pada suhu 30, 70 dan 110°C dan ujian hentaman halaju rendah pada pelbagai tenaga hentaman digunakan untuk pengesahan model berangka. Kod tidak lurus LS-DYNA kemudiannya digunakan untuk membangunkan model unsur terhingga (FE) FML. Model Johnson-Cook, kriteria kegagalan Chang-Chang dan model zon jeleket digunakan untuk mensimulasi masing-masing aluminium, GFRP dan lekangan. Lekangan Mod-I dan Mod-II, dan penebukan kuasi-statik FML pada suhu menaik dimodelkan dan ditentukan. Selepas itu, gabungan analisis aras tenaga hentaman dan suhu telah dilaksanakan menggunakan model sukuan FE. Model penurunan sifat terubahsuai juga digunakan untuk memperoleh sifat pada suhu 50 dan 70°C secara berkesan dengan parameter penentuan tunggal. Dengan menggunakan model FE yang disahkan, kajian berparameter telah dijalankan untuk mengkaji kesan perubahan parameter geometri pada suhu menaik. Keputusan menunjukkan bahawa peningkatan suhu mempengaruhi tindakan hentaman halaju rendah dan rintangan hentaman FML. Peningkatan suhu menjejaskan GFRP dan permukaan GFRP/aluminium dengan lebih ketara berbanding dengan aluminium. Penurunan prestasi FML adalah berterusan yang mana ia dilihat kurang ketara pada suhu 30 hingga 70°C, namun, didapati ketara pada suhu 70 hingga 110°C. Oleh itu, kaedah pemodelan FE yang dicadangkan menyediakan kaedah untuk simulasi, meramalkan dan menganalisis hentaman FML dengan pertimbangan kesan suhu. Penyelidikan ini menyumbang kepada pemajuan FML dan komposit untuk penggunaan pada suhu tinggi. Kaedah FE menyediakan cara yang jelas dan bolehharap untuk mensimulasi dan menganalisis prestasi hentaman FML pada keadaan suhu yang berbeza.

TABLE OF CONTENTS

	TITLE	PAGE
	DECLARATION	ii
	DEDICATION	iii
	ACKNOWLEDGEMENT	iv
	ABSTRACT	v
	ABSTRAK	vi
	TABLE OF CONTENTS	vii
	LIST OF TABLES	xiv
	LIST OF FIGURES	xvi
	LIST OF ABBREVIATIONS	xxvi
	LIST OF SYMBOLS	xxvii
CHAPTER 1	INTRODUCTION	1
	1.1 Research Background	1
	1.2 Problem Statement	3
	1.3 Objective	3
	1.4 Scopes of Study	4
	1.5 Significance of Research	5
	1.6 Thesis Chapter Summary	6
CHAPTER 2	LITERATURE REVIEW	9
	2.1 Origin of Fibre Metal Laminates (FMLs)	9
	2.1.1 Development of Composite Laminates	9
	2.1.2 Development of FMLs	10
	2.2 Advantages of FML	12
	2.3 Factors that Influence the Performance of FMLs	13
	2.3.1 Metal Composition	14
	2.3.2 Fibre Material Types	15
	2.3.3 Fibre and Layup Orientation	16

2.3.4	Resin Types	18
2.3.5	Thickness Distribution	19
2.3.6	Metal Volume Fraction	20
2.3.7	Fibre Volume Fraction	21
2.3.8	Laminate Bonding Strength	21
2.4	Fabrication of FMLs	22
2.4.1	Surface Preparations	22
2.4.2	Fabrication Methods	23
2.4.2.1	Hand Layup	23
2.4.2.2	Vacuum Bagging	24
2.4.2.3	Hot and Cold Press	24
2.4.2.4	Vacuum Infusion Process	24
2.4.2.5	Autoclave	25
2.5	Mechanical Characterisation of FMLs	25
2.5.1	Quasi-Static Perforation	26
2.5.2	Low-Velocity Impact	27
2.5.3	Strain Rate Dependency	28
2.5.4	Fatigue Crack Propagation	30
2.5.5	Interfacial Delamination	30
2.6	Thermal Characterisation	31
2.6.1	Temperature Effect on Aluminium	32
2.6.2	Temperature Effect on Glass Fibre Reinforced Polymer (GFRP)	32
2.6.3	Temperature Effect on Delamination	37
2.6.4	Temperature Effect on FMLs	38
2.6.5	Thermal Fatigue/Shock	41
2.7	Failure Characterisation	42
2.8	Impact Characteristics Evaluation	45
2.8.1	Load Response	45
2.8.2	Velocity Response	46
2.8.3	Energy Response	47
2.8.4	Deformation	48
2.9	FML Study Design Methods	48
2.9.1	Analytical Method	48

2.9.2	Experimental Method	51
2.9.3	Numerical Method	52
2.9.3.1	Element Formulation	53
2.9.3.2	Material Models and Failure Criterion	55
2.9.3.3	Delamination Modelling	57
2.9.3.4	Perforation and Impact Modelling of FML	60
2.10	Summary of findings	61
2.11	Research Gap	62
CHAPTER 3	RESEARCH METHODOLOGY	63
3.1	Introduction	63
3.2	Material Selection and Acquisition	65
3.3	Experimental Investigation of GFRP Composite	66
3.3.1	GFRP Specimen Preparation	68
3.3.2	GFRP Laminated Aluminium Specimen Preparation	71
3.3.3	Experimental Setup	74
3.4	Experimental Tests on FMLs	77
3.4.1	FML Panel Fabrication	77
3.4.2	Experimental Setup	80
3.4.2.1	Quasi-Static Tests	80
3.4.2.2	Low-Velocity Impact Tests	82
3.5	Finite Element Method	85
3.5.1	Model Assumption	86
3.5.2	Modelling Approach and Validation	87
3.5.3	Software Implemented	88
3.5.4	Material Modelling Constitutive Equations	89
3.5.4.1	Aluminium Material Modelling	89
3.5.4.2	GFRP Material Modelling	90
3.5.4.3	Cohesive Zone Modelling	92
3.5.5	Mesh Convergence	94
3.5.6	Main study approach on impact energy levels and temperature	94
3.5.7	Parametric Study Approach	96

CHAPTER 4	TEMPERATURE CHARACTERISATION ON MECHANICAL AND DELAMINATION PROPERTIES OF FMLS	99
4.1	Introduction	99
4.2	Data Analysis Methodology	100
4.3	Mechanical Properties of GFRP	100
4.3.1	Tensile Tests	101
4.3.2	Compression Tests	110
4.3.3	Shear Tests	116
4.3.4	Summary	119
4.4	Delamination Properties of GFRP Laminated Aluminium	121
4.4.1	Double Cantilevered Beam Tests	121
4.4.2	End Notched Flexural Tests	123
4.4.3	Data Reduction	125
4.4.4	Summary	127
4.5	Empirical Modelling	128
4.5.1	Comparison of Models	131
4.5.2	Literature Data Fitting	140
4.6	Summary	144
CHAPTER 5	TEMPERATURE CHARACTERISATION ON QUASI-STATIC AND LOW-VELOCITY IMPACT RESPONSE OF FML PANELS	147
5.1	Introduction	147
5.2	Quasi-Static Indentation Tests on FMLs	147
5.2.1	Temperature Effect on Loading and Energy Absorption Response of FMLs	148
5.2.2	Quasi-static Damage Response of FMLs at Different Temperatures	151
5.2.3	Empirical Curve Fitting	154
5.3	Low-velocity Impact Tests on FMLs	156
5.3.1	Load-Displacement and Energy Absorption Response of FMLs	157

	5.3.2	Damage Response of FMLs	162
5.4		Summary	169
CHAPTER 6		FINITE ELEMENT ANALYSES AND VALIDATION OF	
		TEMPERATURE EFFECT ON FMLS	173
6.1		Introduction	173
6.2		Material Modelling Details	173
	6.2.1	Johnson-Cook Model	173
	6.2.2	Chang-Chang Failure Model	175
	6.2.3	Cohesive Zone Model	176
6.3		FE Analyses of Interlaminar Delamination	179
	6.3.1	Model Setup	179
	6.3.2	Mesh Convergence Study	182
	6.3.3	Numerical Validation and Analyses	184
	6.3.4	Crack Initiation and Stress Distribution	188
	6.3.5	Summary	193
6.4		FE Analyses of Quasi-Static Perforation	195
	6.4.1	Model Setup	195
	6.4.2	Numerical Validation and Analyses of Temperature Effect	198
	6.4.3	Damage Morphologies Evaluation	208
	6.4.4	Summary	211
6.5		FE Analyses of Low-Velocity Impact	213
	6.5.1	Model Setup	213
	6.5.2	Quarter and Half Model Validation with Impact Energy Level	215
		6.5.2.1 Load-Displacement Plot Analysis and Validation	215
		6.5.2.2 Impact Characteristics Analysis and Validation	218
		6.5.2.3 Post Impact Damage Analysis	221
		6.5.2.4 FML Deflection Analysis	230
	6.5.3	Combined Effect of Impact Energy Levels and Temperature	233

6.5.3.1	Load-Displacement Responses	234
6.5.3.2	Velocity-Displacement Responses	238
6.5.3.3	Energy-Time Responses	242
6.5.3.4	Final Deflection of FMLs Across the Symmetry	245
6.5.3.5	Impact Characteristics Analyses	249
6.5.4	Summary	256
CHAPTER 7	PARAMETRIC STUDIES OF FMLS	259
7.1	Introduction	259
7.2	Effects of Impactor Diameter and Clamped Opening Diameter on FML Damage	260
7.2.1	History Plot Analysis	260
7.2.1.1	Load-Displacement Responses	260
7.2.1.2	Velocity-Displacement Responses	265
7.2.1.3	Energy-Time Responses	268
7.2.1.4	Final Deflection of FMLs Across the Symmetry	271
7.2.2	Impact Characteristics Analyses	274
7.3	Effects of Aluminium and GFRP Thickness on FML Damage	279
7.3.1	History Plot Analysis	279
7.3.1.1	Load-Displacement Responses	280
7.3.1.2	Velocity-Displacement Responses	281
7.3.1.3	Energy-Time Responses	282
7.3.1.4	Final Deflection of FMLs Across the Symmetry	283
7.3.2	Impact Characteristics Analyses	283
7.4	Summary	286
CHAPTER 8	CONCLUSIONS AND RECOMMENDATIONS	289
8.1	Research Outcomes	289
8.2	Contributions to Knowledge	291
8.3	Future Works	292

REFERENCES	294
Appendix A Curve fitting for Chang-Chang properties	308
Appendix B Curve fitting for cohesive zone model	309
LIST OF PUBLICATIONS	310

LIST OF TABLES

TABLE NO.	TITLE	PAGE
Table 3.1	Specification details of experimental test specimens based on ASTM.	73
Table 3.2	Details of low-velocity impact test parameters.	85
Table 3.3	FE study on combinations of impact energy level and temperature.	95
Table 3.4	Parametric study on combinations of impactor diameter and clamped opening diameter.	97
Table 3.5	Details of FML mass with different combinations of aluminium and GFRP thickness.	98
Table 4.1	Results of properties at each temperature from mechanical tests (with standard deviation and coefficient of variance).	120
Table 4.2	Results of properties at each temperature from delamination tests (with standard deviation and coefficient of variance).	128
Table 4.3	Fitted parameters of the empirical models for each property.	139
Table 4.4	Fitted parameters of the empirical models for literature data.	143
Table 5.1	Results of peak load and total energy absorbed at each temperature of quasi-static perforation tests (with standard deviation and coefficient of variance).	151
Table 5.2	Fitted parameters of the empirical models for each property.	156
Table 5.3	Recovery distance at each impact energy.	160
Table 5.4	Results of peak load and total energy absorbed at each impact energy of low-velocity impact tests (with standard deviation).	161

Table 6.1	Material properties of aluminium 2024-T3 for Johnson-Cook material model.	174
Table 6.2	Material properties of aluminium in the references.	174
Table 6.3	Material properties of GFRP for Chang-Chang failure criterion.	175
Table 6.4	Mode-I and Mode-II delamination properties at each temperature.	176
Table 6.5	Material properties of the cohesive model.	178
Table 6.6	Mode-I slope and peak load data comparison between experimental and simulation results.	186
Table 6.7	Mode-II slope and peak load data comparison between experimental and simulation results.	188
Table 6.8	Peak load values of FML panels at each impact energy from experiment, FE quarter and half models.	219
Table 6.9	Total energy absorption of FML panels at each energy from experiment, FE quarter, and half models.	220
Table 6.10	Total energy absorption values of FML panels under different impact energy and temperature.	250
Table 6.11	ERC values of FML panels under different impact energy and temperature.	252
Table 6.12	Peak load values of FML panels under different impact energy and temperature.	254
Table 6.13	Percentage rebound values of FML panels under different impact energy and temperature.	256
Table 7.1	FML impact characteristics under different impactor diameter and clamped opening diameter.	278
Table 7.2	FML impact characteristics across varying thickness ratio, φ .	286

LIST OF FIGURES

FIGURE NO.	TITLE	PAGE
Figure 1.1	Cross-section of a typical FML.	1
Figure 1.2	Large commercial aircraft - Airbus A3XX.	2
Figure 2.1	Comparison of perforation energy between aluminium 2024-T3, GLARE, ARALL, and CFRP.	11
Figure 2.2	Comparison of perforation energy between FML of 2024-T3, 2024-O aluminium, and plain composite with increasing composite thickness.	14
Figure 2.3	Effect of thickness and number of layup on perforation energy.	19
Figure 2.4	Tensile strength vs strain rate of ARALL 1, GLARE 3, and Aluminum 7075-T6.	29
Figure 2.5	Strength vs strain rate for tensile and compressive tests on UD GFRP.	29
Figure 2.6	Effects of temperature on the threshold impact energy of GFRP with different surface treatments of silane coupling agents: ○, 0.01wt% γ -MPS; △, 0.4wt% γ -MPS; □, 1.0wt% γ -MPS; ●, methanol washed 0.4wt% γ -MPS; ▲, 0.4 wt.% γ -GPS.	36
Figure 2.7	Tensile strength and interlaminar shear strength vs temperature of PEEK FML.	39
Figure 2.8	Comparison between ultimate shear strength of FML specimens that are not exposed, exposed to 1000 cycles and 2000 cycles of -50 to 80°C.	42
Figure 2.9	Fibre bridging mechanism by fibre epoxy layer in FMLs.	43
Figure 2.10	Low-velocity impact failure process: (a) Indentation, (b) Partial Perforation, (c) Full Perforation, and (d) Penetration.	44

Figure 2.11	Typical load-displacement response of FML under low-velocity impact.	46
Figure 2.12	Comparisons between solid element and shell element FE models with respect to impact tests at predicting load and energy curves.	54
Figure 3.1	Methodology process flowchart.	64
Figure 3.2	Schematic of (a) T-0, (b) T-90, (c) C-0, (d) C-90, and (e) S specimens with their respective fibre orientations and dimensions.	68
Figure 3.3	Specimens with tabs (black) and strain gauges installed. (From top to bottom: tensile 0°, tensile 90°, and shear specimens.)	69
Figure 3.4	Schematic diagram of combined loading compression fixture.	71
Figure 3.5	Shimadzu AG-X plus universal testing machine.	74
Figure 3.6	Compression jig setup.	75
Figure 3.7	Setup of GFRP laminated aluminium for DCB test: (a) schematic diagram, (b) actual setup	76
Figure 3.8	Setup of GFRP laminated aluminium for ENF test: (a) schematic diagram, (b) actual setup	76
Figure 3.9	FML layup specifications	78
Figure 3.10	FML fabrication process	79
Figure 3.11	Quasi-static test setup with Shimadzu testing machine.	81
Figure 3.12	CEAST 9350 drop impact testing machine for low-velocity impact test.	83
Figure 3.13	Low-velocity impact test specifications.	84
Figure 3.14	Bilinear traction separation law.	92
Figure 4.1	Tensile stress versus axial tensile strain curves of T-0 specimens at (a) 30, (b) 70, and (c) 110°C.	102
Figure 4.2	Tensile stress versus lateral tensile strain curves of T-0 specimens at (a) 30, (b) 70, and (c) 110°C.	104
Figure 4.3	Failure mode of T-0 specimen.	104

Figure 4.4	Average longitudinal tensile modulus, E_A and strength, X_T versus temperature (with standard deviation) of T-0 specimens.	105
Figure 4.5	Averaged longitudinal Poisson's ratio, ν_{AB} versus temperature (with standard deviation) of T-0 specimens.	106
Figure 4.6	Tensile stress versus strain curves of T-90 specimens at (a) 30, (b) 70, and (c) 110°C.	107
Figure 4.7	Average transverse tensile modulus, E_B and strength, Y_T versus temperature (with standard deviation) of T-90 specimens.	108
Figure 4.8	Failure mode of T-90 specimens tested at (a) 30, (b) 70, and (c) 110°C.	109
Figure 4.9	Compressive stress versus strain curves of C-0 specimens at (a) 30, (b) 70, and (c) 110°C.	111
Figure 4.10	Average longitudinal compressive modulus, E_A^C and strength, X_C versus temperature (with standard deviation) of C-0 specimens.	112
Figure 4.11	Failure mode of C-0 specimens tested at (a) 30, (b) 70, and (c) 110°C.	113
Figure 4.12	Compressive stress versus strain curves of C-90 specimens at (a) 30, (b) 70, and (c) 110°C.	114
Figure 4.13	Averaged transverse compressive modulus, E_B^C and strength, Y_C versus temperature (with standard deviation) of C-90 specimens.	115
Figure 4.14	Failure mode of C-90 specimen.	116
Figure 4.15	Shear stress versus strain curves of S specimens at (a) 30, (b) 70, and (c) 110°C.	117
Figure 4.16	Average in-plane shear modulus, G_{AB} and strength, S_C versus temperature (with standard deviation) of S specimens.	118
Figure 4.17	Load versus displacement curves of DCB specimens at (a) 30, (b) 70, and (c) 110°C.	122

Figure 4.18	Load versus displacement curves of ENF specimens at (a) 30, (b) 70, and (c) 110°C.	124
Figure 4.19	Average Mode-I modulus and fracture toughness versus temperature (with standard deviation) of DCB specimens.	126
Figure 4.20	Average Mode-II modulus and fracture toughness versus temperature (with standard deviation) of ENF specimens.	127
Figure 4.21	Wong's model parameter indicating the temperature sensitivity of the property.	130
Figure 4.22	Normalised (a) E_A and (b) X_T versus temperature with experimental test data and empirical curves.	132
Figure 4.23	Normalised (a) E_B and (b) Y_T versus temperature with experimental test data and empirical curves.	132
Figure 4.24	Normalised (a) E_A^C and (b) X_C versus temperature with experimental test data and empirical curves.	133
Figure 4.25	Normalised (a) E_B^C and (b) Y_C versus temperature with experimental test data and empirical curves.	134
Figure 4.26	Normalised (a) G_{AB} and (b) S_C versus temperature with experimental test data and empirical curves.	134
Figure 4.27	Normalised (a) E_{IC} and (b) G_{IC} versus temperature with experimental test data and empirical curves.	135
Figure 4.28	Normalised (a) E_{IIC} and (b) G_{IIC} versus temperature with experimental test data and empirical curves.	136
Figure 4.29	Normalised tensile strength versus temperature results by Correia et al. with fitted model.	141
Figure 4.30	Normalised shear strength versus temperature results by Rosa et al. with fitted model.	141
Figure 4.31	Normalised tensile strength versus temperature results by Lu et al. with fitted model.	141
Figure 4.32	Normalised tensile strength versus temperature results by Gibson et al. with fitted model.	142
Figure 5.1	Load versus displacement curves of FML quasi-static perforation specimens at (a) 30, (b) 70, and (c) 110°C.	149

Figure 5.2	Averaged peak load and total energy absorbed versus temperature (with standard deviation) of quasi-static perforation specimens.	151
Figure 5.3	Top (left) and rear (right) side of FML panels after quasi-static indentation tests at (a) 30, (b) 70, and (c) 110°C.	152
Figure 5.4	Cross-section of FML panel after test (110°C).	154
Figure 5.5	Normalised quasi-static FML (a) peak load and (b) total energy absorbed versus temperature with experimental test data and empirical curves.	155
Figure 5.6	Load versus displacement curves of FML low-velocity impact specimens at (a) 5, (b) 8, (c) 10, (d) 12, (e) 13.5, and (f) 15 J.	159
Figure 5.7	Averaged peak load and total energy absorbed versus temperature (with standard deviation) of low-velocity impact specimens.	161
Figure 5.8	Damage morphologies of FML panels at 5 J on (a) Top surface, (b) rear surface, and (c) cross-section. (continued)	163
Figure 5.9	Damage morphologies of FML panels at 8 J on (a) Top surface, (b) rear surface, and (c) cross-section.	164
Figure 5.10	Damage morphologies of FML panels at 10 J on (a) Top surface, (b) rear surface, and (c) cross-section.	165
Figure 5.11	Damage morphologies of FML panels at 12 J on (a) Top surface, (b) rear surface, and (c) cross-section.	167
Figure 5.12	Damage morphologies of FML panels at 13.5 J on (a) Top surface, (b) rear surface, and (c) cross-section.	168
Figure 5.13	Damage morphologies of FML panels at 15 J on (a) Top surface, (b) rear surface, and (c) cross-section.	169
Figure 6.1	FE model discretisation of (a) Mode-I and (b) Mode-II delamination, (c) elements close-up arrangement between aluminium, cohesive, and GFRP.	180
Figure 6.2	Effect of the Mesh size on Mode-I load-displacement curves.	183
Figure 6.3	Slope values of load-displacement versus mesh sizes.	183

Figure 6.4	Mode-I load-displacement curves validation between experiment and simulation at (a) 30, (b) 70, and (c) 110°C.	185
Figure 6.5	Mode-II load-displacement curves validation between experiment and simulation at (a) 30, (b) 70, and (c) 110°C.	187
Figure 6.6	Mode-I crack front stress distributions at (a) 30, (b) 70, and (c) 110°C. (c.t. refers to location of crack tip)	189
Figure 6.7	Normalised Mode-I stress distributions along the crack front at (a) 30, (b) 70, and (c) 110°C.	190
Figure 6.8	Mode-II crack front stress distributions at (a) 30, (b) 70, and (c) 110°C. (c.t. refers to location of crack tip)	192
Figure 6.9	Normalised Mode-II stress distributions along crack tip at (a) 30, (b) 70, and (c) 110°C.	193
Figure 6.10	FE model discretisation of FML layup.	196
Figure 6.11	Half model FE discretisation of FML panel for quasi-static perforation.	197
Figure 6.12	Load-displacement curves of FML panels under quasi-static loading at (a) 30, (b) 70, and (c) 110°C.	200
Figure 6.13	Damage sequence of FE panels at 30°C through load-displacement curve.	202
Figure 6.14	Energy-displacement curves of FML panels under quasi-static loading at (a) 30, (b) 70, and (c) 110°C.	203
Figure 6.15	Total energy absorption of FML panels under quasi-static loading at 30, 70, and 110°C.	204
Figure 6.16	Dissipated energy versus displacement curves of aluminium, GFRP, and cohesive interfaces at (a) 30, (b) 70, and (c) 110°C.	206
Figure 6.17	Total dissipated energy ratio between aluminium, GFRP, and cohesive interface at each temperature.	207
Figure 6.18	Comparison of damage morphologies for FML panels at 30°C - (a) Top view, (b) Bottom and reverse isometric view, and (c) Cross-sectional view.	209

Figure 6.19	Comparison of damage morphologies for FML panels at 70°C - (a) Top view, (b) Bottom and reverse isometric view, and (c) Cross-sectional view.	210
Figure 6.20	Comparison of damage morphologies for FML panels at 110°C - (a) Top view, (b) Bottom and reverse isometric view, and (c) Cross-sectional view.	210
Figure 6.21	Quarter model FE discretisation of FML panel for low-velocity impact test.	215
Figure 6.22	Load-displacement curves of FML panels under low-velocity impacts of (a) 5, (b) 8, (c) 10, (d) 12, (e) 13.5, and (f) 15 J.	217
Figure 6.23	Peak load of FML panels under low-velocity impacts of (a) 5, (b) 8, (c) 10, (d) 12, (e) 13.5, and (f) 15 J.	219
Figure 6.24	Total energy absorption of FML panels under low-velocity impacts of (a) 5, (b) 8, (c) 10, (d) 12, (e) 13.5, and (f) 15 J.	220
Figure 6.25	Experimental versus FE post impact damage analysis under 5 J impact energy.	222
Figure 6.26	Experimental versus FE post impact damage analysis under 8 J impact energy.	224
Figure 6.27	Experimental versus FE post impact damage analysis under 10 J impact energy.	225
Figure 6.28	Experimental versus FE post impact damage analysis under 12 J impact energy.	226
Figure 6.29	Experimental versus FE post impact damage analysis under 13.5 J impact energy.	227
Figure 6.30	Experimental versus FE post impact damage analysis under 15 J impact energy.	229
Figure 6.31	Cross-sectional deflection of FML panels at maximum and final deflection under impact energy of 5, 8, 10, 12, 13.5, and 15 J.	231
Figure 6.32	Effect of the impact energy on the load-displacement curves at (a) 30, (b) 50, (c) 70, (d) 90, and (e) 110°C.	235

Figure 6.33	Effect of increasing temperature on the load-displacement curves at (a) 5, (b) 8, (c) 10, (d) 12, (e) 13.5, and (f) 15 J.	238
Figure 6.34	Effect of the impact energy on the velocity-displacement curves at (a) 30, (b) 50, (c) 70, (d) 90, and (e) 110°C.	239
Figure 6.35	Effect of increasing temperature on the velocity-displacement curves at (a) 5, (b) 8, (c) 10, (d) 12, (e) 13.5, and (f) 15 J.	241
Figure 6.36	Effect of the impact energy on the energy-time curves at (a) 30, (b) 50, (c) 70, (d) 90, and (e) 110°C.	243
Figure 6.37	Effect of increasing temperature on the energy-time curves at (a) 5, (b) 8, (c) 10, (d) 12, (e) 13.5, and (f) 15 J.	244
Figure 6.38	Effect of impact energy on the final deflection of FML panels at (a) 30, (b) 50, (c) 70, (d) 90, and (e) 110°C.	246
Figure 6.39	Effect of increasing temperature on the final deflection of FML panels at (a) 5, (b) 8, (c) 10, (d) 12, (e) 13.5, and (f) 15 J.	248
Figure 6.40	Total energy absorption of FML panels for varying impact energy and temperature.	250
Figure 6.41	ERC of FML panels under different impact loading and temperature.	251
Figure 6.42	The peak load of FML panels under different impact energy and temperature.	253
Figure 6.43	Percentage rebound of FML panels under different impact energy and temperature.	255
Figure 7.1	Effect of the impactor diameter on the load-displacement curves with clamped opening diameter of (a) 80, (b) 100, (c) 127, (d) 140, and (e) 160 mm.	261
Figure 7.2	Effect of the clamped opening diameter on the load-displacement curves with impactor diameter of (a) 8, (b) 10, (c) 12.7, (d) 14, and (e) 16 mm.	264

Figure 7.3	Effect of the impactor diameter on the velocity-displacement curves with clamped opening diameter of (a) 80, (b) 100, (c) 127, (d) 140, and (e) 160 mm.	266
Figure 7.4	Effect of the clamped opening diameter on the velocity-displacement curves with impactor diameter of (a) 8, (b) 10, (c) 12.7, (d) 14, and (e) 16 mm.	268
Figure 7.5	Effect of the impactor diameter on the energy-time curves with clamped opening diameter of (a) 80, (b) 100, (c) 127, (d) 140, and (e) 160 mm.	269
Figure 7.6	Effect of the clamped opening diameter on the energy-time curves with impactor diameter of (a) 8, (b) 10, (c) 12.7, (d) 14, and (e) 16 mm.	271
Figure 7.7	Effect of the impactor diameter on the deflection responses with clamped opening diameter of (a) 80, (b) 100, (c) 127, (d) 140, and (e) 160 mm.	272
Figure 7.8	Effect of the clamped opening diameter on the deflection responses with impactor diameter of (a) 8, (b) 10, (c) 12.7, (d) 14, and (e) 16 mm.	274
Figure 7.9	Total energy absorption of FML panels for varying impactor diameter and clamped opening diameter.	275
Figure 7.10	ERC of FML panels under different impactor diameter and clamped opening diameter.	276
Figure 7.11	The peak load of FML panels under different impactor diameter and clamped opening diameter.	277
Figure 7.12	Percentage rebound of FML panels under different impactor diameter and clamped opening diameter.	278
Figure 7.13	Effect of the thickness ratio, ϕ on the load-displacement curves.	280
Figure 7.14	Effect of the thickness ratio, ϕ on the velocity-displacement curves.	281
Figure 7.15	Effect of the thickness ratio, ϕ on the energy-time curves.	282
Figure 7.16	Effect of the thickness ratio, ϕ on the deflection responses.	283

Figure 7.17	Total energy absorption and ERC of FML panels across varying thickness ratio, φ .	284
Figure 7.18	The peak load of FML panels across varying thickness ratio, φ .	285
Figure 7.19	Percentage rebound of FML panels across varying thickness ratio, φ .	286

LIST OF ABBREVIATIONS

ARALL	-	Aramid Reinforced Aluminium Laminates
ASTM	-	American Society for Testing Methods
BFRP	-	Basalt Fibre Reinforced Polymer
BVID	-	Barely Visible Impact Damage
CARALL	-	Carbon Reinforced Aluminium Laminates
CFRP	-	Carbon Fibre Reinforced Polymer
DCB	-	Double Cantilever Beam
ENF	-	End Notched Flexural
ERC	-	Energy Restitution Coefficient
FE	-	Finite Element
FEM	-	Finite Element Method
FML	-	Fibre Metal Laminates
FRP	-	Fibre Reinforced Polymer
GFRP	-	Glass Fibre Reinforced Polymer
GLARE	-	Glass Laminated Aluminium Reinforced Epoxy
MVF	-	Metal Volume Fraction
PEEK	-	Poly-ether-ether-ketone
UD	-	Unidirectional
3D	-	Three-dimensional
T-0	-	Tensile loaded across 0° fibre direction
T-90	-	Tensile loaded across 90° fibre direction
C-0	-	Compression loaded across 0° fibre direction
C-90	-	Compression loaded across 90° fibre direction
S	-	Shear loaded across $\pm 45^\circ$ fibre direction

LIST OF SYMBOLS

T_g	-	Glass transition temperature
E_{abs}	-	Energy absorbed
E_{imp}	-	Impact energy
F_P	-	Peak load
L	-	Length
W	-	Width
h, t	-	Thickness/Height
K	-	stiffness
a_o	-	Initial crack lengths
L	-	Half-span length in ENF setup
ρ	-	Density
E	-	Young's modulus
G	-	Shear modulus
N	-	Poisson's ratio
σ_y	-	Flow stress
A, B, n	-	Johnson-Cook plastic strain material constant
C	-	Johnson-Cook strain rate effect constant
M	-	Johnson-Cook temperature effect constant
$\bar{\epsilon}_p$	-	Effective plastic strain
$\dot{\epsilon}$	-	Effective total strain rate
$\dot{\epsilon}_0$	-	Quasi-static threshold rate
T	-	Effective room temperature
T_{room}	-	Room temperature
T_{melt}	-	Melting point
d_1, d_2, d_3	-	Johnson-Cook pressure effect constants
d_4	-	Johnson-Cook strain rate effect constant
d_5	-	Johnson-Cook temperature effect constant
η	-	Ratio between pressure and effective stress
e_f	-	Tensile fibre failure mode
e_c	-	Compressive fibre failure mode

e_m	-	Tensile matrix failure mode
e_d	-	Compressive matrix failure mode
σ_1	-	Effective stress tensor components in fibre direction
σ_2	-	Effective stress tensor components in matrix direction
τ_{12}	-	Effective shear tensor
X_T	-	Longitudinal tensile strength
X_C	-	Longitudinal compressive strength
Y_T	-	Transverse tensile strengths
Y_C	-	Transverse compressive strengths
S_C	-	Shear strength
E_A	-	Longitudinal Young's modulus
E_B	-	Transverse Young's modulus
E_A^C	-	Longitudinal compressive Young's modulus
E_B^C	-	Transverse compressive Young's modulus
G_{AB}	-	Shear modulus
ν_{BA}, ν_{AB}	-	In plane Poisson's ratio
B	-	Weighting factor for the shear term
ε_1	-	Axial tensile strain
ε_2	-	Lateral tensile strain
γ_{12}	-	Shear strain
G_{IC}	-	Mode-I energy release rate
σ	-	Normal direction peak traction
δ_N	-	Normal direction ultimate displacement
E_N	-	Mode-I penalty stiffness
G_{IIC}	-	Mode-II energy release rate
τ	-	Tangential direction peak traction
δ_T	-	Tangential direction ultimate displacement
E_T	-	Mode-II penalty stiffness
δ^0	-	Mixed-mode damage initiation displacement
δ_I	-	Normal separation
δ_{II}	-	Tangential separation
δ_I^0	-	Mode-I damage initiation separation
δ_{II}^0	-	Mode-II damage initiation separation

δ^F	-	Mixed-mode displacement
ψ	-	Mode mixity
XMU	-	Mixed-mode criteria stiffness
E_{IC}	-	Back-calculated Mode-I modulus
E_{IIC}	-	Back-calculated Mode-II modulus
k_I	-	Mode-I stiffness
k_{II}	-	Mode-II stiffness
Γ_I	-	Mode-I compliance
Γ_{II}	-	Mode-II compliance
$P(T)$	-	Material property at effective temperature
P_{min}	-	Material property at minimum temperature
P_{max}	-	Material property at maximum temperature
T_{min}	-	Minimum temperature
T_0, m_0	-	Mahieux model parameters
k', T_x	-	Gibson model parameters
M, N	-	Correia model parameters
Z	-	Current (modified Wong) model parameter
Φ	-	Thickness ratio between aluminium and GFRP

CHAPTER 1

INTRODUCTION

1.1 Research Background

In the recent decades, fibre metal laminates (FMLs) have become one of the major interesting research subjects. This is due to increasing requirement for superior lightweight, durable, and damage tolerant materials by particularly aircraft and aerospace industries. The substantial development of FMLs started at Fokker/TU Delft in the Netherlands, during the late 1970s. Typically, it has been suggested that thin sheets of metal alloy are laminated with alternating composite layers to form a laminated sandwich structure, as shown in Figure 1.1.

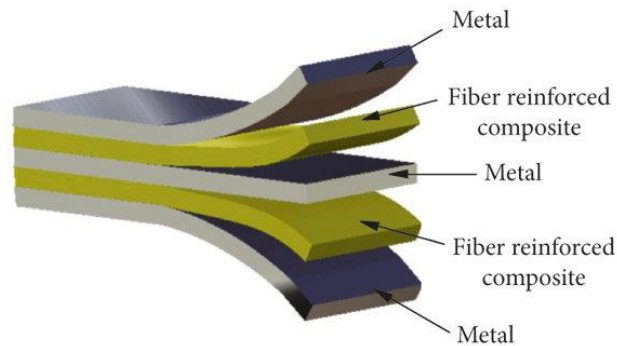


Figure 1.1 Cross-section of a typical FML [1].

The usefulness of structural materials depends on their ability to withstand damage, fracture, and failure. Damage is a broad term used to define when a material or structure loses some integrity that decreases its ability to function. Damage can range from minor to large scale impairment and can be caused by a large variety of different sources. Hence, the term ‘damage’ can be used in any part where impairment is involved. Meanwhile, fracture is more specific, which is defined by when a structure cracks, and is broken off physically, either into smaller pieces or into two separate

parts. Finally, failure is the condition when a said material or structure completely loses its intended function. Therefore, damage, fracture, and failure are often related to each other. Increasing damage typically leads to failure, but do not always cause fracture, depending on the type of damage. Moreover, fracture in materials is also usually a form of damage.

FML is a better substitute material for aircraft structures. These advantages will help towards developing of much larger aircrafts such as the Airbus A3XX shown in Figure 1.2 [2]. It has been increasingly found in aeronautical, marine, and automobile applications. The glass laminate aluminium reinforced epoxy (GLARE) variant of FML has been used prevalently in aircraft structures, most notably the fuselage and tail units of Airbus A380 [2, 3].



Figure 1.2 Large commercial aircraft - Airbus A3XX [2].

GLARE has the potential to be used at elevated temperatures owing to the heat resistance of the glass fibres. Previous reports indicate potential use of FMLs as fire retardants and thermal resistors [4, 5]. A vital feature of aircraft crashworthiness is to consider the fire resistance of fuselage skin materials. That is, in the event of aircraft catching fire, there is very short escape time, especially for large passenger aircrafts (>500 passengers). There is a possibility to expand the use of FML into other applications that requires energy absorption and impact absorption at elevated temperature. For instance, aircraft turbine and exhausts, supersonic aircraft structures, aerospace structures, and even advanced automobile structures often operates at high temperature and impact prone conditions.

1.2 Problem Statement

Material strength generally degrades due to rise of temperature; therefore, it is imperative to probe the extent of strength reduction on FML. Furthermore, the low-velocity impact response of FML could be significantly exacerbated at high temperature and must be investigated. What is the low-velocity impact response of FML at higher temperature? The effects of temperature towards the low-velocity impact response of FMLs are still sparse, and limited finding is only available in the general literature. Thermal stress and strains are common in aircraft structure and FML operating conditions. Metal and composite as constituents of FMLs are both temperature dependent. For instance, even when the strength of FML is good, the structure may be significantly affected by temperature.

Furthermore, impact damage causes 13% of the total repair done on the primary structure of Boeing 747 [2], and this raises concerns on the costs required ascribed to impact. There are vast possible combinations for the relatively new FML, which makes research difficult in terms of cost, time, and waste. Hence, more research is much needed to expand this field. Many studies have studied the low-velocity impact of FMLs using FE analyses, while there is currently no known investigation that includes temperature effect. The effects of temperature on the low-velocity impact response, morphology, and characteristics of FML are currently unknown.

1.3 Objective

The aim of this research is to evaluate the low-velocity impact characteristics of FML under high temperatures. The objectives are:

1. To simulate the low-velocity impact response of FML at high temperatures by utilising FE model.
2. To validate the FE models with experimental results at each temperature.
3. To perform experimental tests and implement empirical model to obtain material properties at each temperature.

4. To characterise the property degradation for FE model inputs using empirical model.
5. To examine the effects of geometrical changes on low-velocity impact at elevated temperature.

1.4 Scopes of Study

The study focuses on temperatures of 30, 70, and 110°C in experimental tests and FE validation. After validation, FE analysis on temperature effects are performed on 30, 50, 70, 90, and 110°C to scrutinise temperature effect. Temperatures below 30 and above 110°C are not covered in this research. The extent of high temperature in this study only reaches until the temperature of 110°C.

The study covers on materials including glass fibre reinforced polymer (GFRP), GFRP laminated aluminium, and glass laminated aluminium reinforced epoxy. The aluminium used is 2024-T3 grade aluminium. The GFRP is S2 grade unidirectional glass fibres prepreg with glass transition temperature (T_g) of 125°C and adhesive epoxy with T_g of 130°C. Other grades of aluminium and types of composites are not analysed. The fabrication process includes oven bonding and hand layup techniques.

The experimental tests include tensile, compression, and shear tests for properties extraction, along with double cantilever beam (DCB) and end notched flexural (ENF) tests for properties extraction and validation. Furthermore, quasi-static indentation tests and low-velocity impact tests were conducted for validation. All experimental tests are conducted in quasi-static rates of loading, except for low-velocity impact tests at impact energies of 5, 8, 10, 12, 13.5, and 15 J. Higher rates of loading and fatigue loading types are not focused on.

The numerical method consists of DCB and ENF FE models, quasi-static, and low-velocity impact models all of which simulated at temperatures of 30, 70, and 110°C. The material models used in FE modelling include Johnson-Cook material model, Chang-Chang failure criteria, and Cohesive Zone Modelling. The FE models

are also modelled in half and quarter models. The parameters used for validation comprise of load-extension curves, peak loads, and slopes for DCB and ENF. Meanwhile, the validation parameters include load-displacement, damage morphology, and total energy absorption for quasi-static and low-velocity impact model.

The main study of this research includes combined analysis between impact energy of 5, 8, 10, 12, 13.5, and 15 J with temperatures 30, 50, 70, 90, and 110°C. The research also incorporates parametric studies on: first, the joint effects of impactor diameter 8, 10, 12.7, 14, and 16 mm with clamped opening diameter of 80, 100, 127, 140, and 160 mm. Secondly, the thickness ratio between aluminium and GFRP with fixed total mass of FML were investigated. Based on the validation of the FE quarter and half models, quarter model is used to simulate parametric study at 10 J based on the design limitation.

1.5 Significance of Research

Research on low-velocity impact of FMLs under high temperatures can bring much understanding, information, and improvements on the material and domain of composites. This can also ensure aeronautical and aerospace structures much safer and reliable. The methodology used in this study will provide insight on the ways of analysing performances of FMLs. The results from experimental tests provide means of creating relation or chart on temperature effect towards composite and delamination parameters for implementing them into FE models. The parametric studies on different impactor diameter, clamped opening diameter, and individual thickness of aluminium and GFRP will generate more practical and beneficial information of FMLs in different applications. Finally, the outcome of the research may facilitate the application of FML under higher temperature condition.

1.6 Thesis Chapter Summary

As presented in Chapter 1, the introduction included the background and the motivations of this study. The problem statement, main aim, objectives, and scopes of study were established. Then, the significance of this research was described.

Chapter 2 is the literature review of this research based on previous researchers. The literatures consist of the development of composite and FML structures, the scrutinization of the factors that contribute towards the composition, and the performance of FMLs. The next part involves the fabrication methods of FMLs in literature. Next, the focus turns on mechanical and thermal factors that affect FML during its operational conditions, how damage occurs, and how to evaluate them. Finally, the methods of study on FML are probed.

Chapter 3 is the methodology of this research. It consists of the material selection, material acquisition, preparation of the specimens. Specimens include GFRP, GFRP laminated aluminium, and FML. Subsequently, the experimental setup for each test are described in detail. Then, FE methodology from the model simplification, approach, and validation are outlined. The material models implemented in this study are also presented. The planning of parametric study is also covered.

Chapter 4 is the experimental results of the tensile, compression, and shear tests on GFRP, then followed by the DCB and ENF results. Furthermore, an empirical curve fitting model is implemented to study and fit the trend of each properties from the experimental results. There is also comparison with some examples from literature.

Chapter 5 detailly describes the results from quasi-static indentation tests and low-velocity impact tests on FMLs. The load-displacement curves are examined to analyse the effects of temperature and impact energy. The damage response is also compared.

Chapter 6 focuses on the detail of modelling each of the FE models, their respective validations, and results. The input of properties for the material models are

described in detail. Then, delamination, quasi-static, and low-velocity impact models are presented in depth, first with the model setup, followed by the mesh convergence study. The validation of each model is shown based on the impact characteristics along with damage morphologies. Most importantly, the main results of combined effects between impact energy and temperatures are examined.

In Chapter 7, the parametric studies of geometrical properties of the FML under low-velocity impact at high temperature are presented. The first part consists of the parametric study outcome of impactor diameter and clamped opening diameter. Next, the second part involves the results from simulation different thickness ratio of aluminium and GFRP.

Lastly, Chapter 8 is the conclusion and recommendations of this research. The main research outcomes are demonstrated, followed by the major contributions towards knowledge in this field. The future works that might stem from this study are also established.

REFERENCES

- [1] Chen, Y., Wang, Y., and Wang, H. Research Progress on Interlaminar Failure Behavior of Fiber Metal Laminates. *Advances in Polymer Technology*, 2020; 2020: p. 3097839.
- [2] Vogelesang, L.B. and Vlot, A. Development of fibre metal laminates for advanced aerospace structures. *Journal of Materials Processing Technology*, 2000; 103(1): p. 1-5.
- [3] Bieniaś, J., Jakubczak, P., and Surowska, B., *11 - Properties and characterization of fiber metal laminates*, in *Hybrid Polymer Composite Materials*, V.K. Thakur, M.K. Thakur, and A. Pappu, Editors. 2017, Woodhead Publishing. p. 253-277.
- [4] Asundi, A. and Choi, A.Y.N. Fiber metal laminates: An advanced material for future aircraft. *Journal of Materials Processing Technology*, 1997; 63(1–3): p. 384-394.
- [5] Roebroeks, G.H.J.J. Fibre-metal laminates: Recent developments and applications. *International Journal of Fatigue*, 1994; 16(1): p. 33-42.
- [6] Correia, J.R., Gomes, M.M., Pires, J.M., and Branco, F.A. Mechanical behaviour of pultruded glass fibre reinforced polymer composites at elevated temperature: Experiments and model assessment. *Composite Structures*, 2013; 98: p. 303-313.
- [7] Elanchezhian, C., Ramnath, B.V., and Hemalatha, J. Mechanical behaviour of glass and carbon fibre reinforced composites at varying strain rates and temperatures. *Procedia Materials Science*, 2014; 6: p. 1405-1418.
- [8] Aydın, F. Effects of various temperatures on the mechanical strength of GFRP box profiles. Vol. 127. 2016. 843-849.
- [9] Karakuzu, R., Erbil, E., and Aktas, M. Impact characterization of glass/epoxy composite plates: An experimental and numerical study. *Composites Part B: Engineering*, 2010; 41(5): p. 388-395.
- [10] Sayer, M., Bektaş, N.B., and Sayman, O. An experimental investigation on the impact behavior of hybrid composite plates. *Composite Structures*, 2010; 92(5): p. 1256-1262.
- [11] Sinmazçelik, T., Avcu, E., Bora, M.Ö., and Çoban, O. A review: Fibre metal laminates, background, bonding types and applied test methods. *Materials & Design*, 2011; 32(7): p. 3671-3685.
- [12] Vlot, A. Impact loading on fibre metal laminates. *International Journal of Impact Engineering*, 1996; 18(3): p. 291-307.
- [13] Vlot, A., Gunnink, J.W., and SpringerLink (Online service). *Fibre metal laminates an introduction*. 2001, Springer Netherlands, Dordrecht. p. 1 online resource.
- [14] Vlot, A. Impact properties of fibre metal laminates. *Composites Engineering*, 1993; 3(10): p. 911-927.
- [15] Vlot, A., Vogelesang, L.B., and Vries, T.J.d. Towards application of fibre metal laminates in large aircraft. *Aircraft Engineering and Aerospace Technology*, 1999; 71(6): p. 558-570.
- [16] Chai, G.B. and Manikandan, P. Low velocity impact response of fibre-metal laminates – A review. *Composite Structures*, 2014; 107: p. 363-381.

- [17] Lawcock, G.D., Ye, L., Mai, Y.W., and Sun, C.T. Effects of fibre/matrix adhesion on carbon-fibre-reinforced metal laminates—II. impact behaviour. *Composites Science and Technology*, 1998; 57(12): p. 1621-1628.
- [18] Li, C.F., Hu, N., Yin, Y.J., Sekine, H., and Fukunaga, H. Low-velocity impact-induced damage of continuous fiber-reinforced composite laminates. Part I. An FEM numerical model. *Composites Part A: Applied Science and Manufacturing*, 2002; 33(8): p. 1055-1062.
- [19] Nakatani, H., Kosaka, T., Osaka, K., and Sawada, Y. Damage characterization of titanium/GFRP hybrid laminates subjected to low-velocity impact. *Composites Part A: Applied Science and Manufacturing*, 2011; 42(7): p. 772-781.
- [20] Sadighi, M., Alderliesten, R.C., and Benedictus, R. Impact resistance of fiber-metal laminates: A review. *International Journal of Impact Engineering*, 2012; 49: p. 77-90.
- [21] Wu, G., Yang, J.-M., and Hahn, H.T. The impact properties and damage tolerance and of bi-directionally reinforced fiber metal laminates. *Journal of Materials Science*, 2007; 42(3): p. 948-957.
- [22] Schijve, J., Van Lipzig, H.T.M., Van Gestel, G.F.J.A., and Hoeymakers, A.H.W. Fatigue properties of adhesive-bonded laminated sheet material of aluminum alloys. *Engineering Fracture Mechanics*, 1979; 12(4): p. 561-579.
- [23] Mitrevski, T., Marshall, I.H., and Thomson, R. The influence of impactor shape on the damage to composite laminates. *Composite Structures*, 2006; 76(1–2): p. 116-122.
- [24] Daiyan, H., Andreassen, E., Grytten, F., Lyngstad, O.V., Luksepp, T., and Osnes, H. Low-velocity impact response of injection-moulded polypropylene plates – Part 1: Effects of plate thickness, impact velocity and temperature. *Polymer Testing*, 2010; 29(6): p. 648-657.
- [25] Daiyan, H., Andreassen, E., Grytten, F., Lyngstad, O.V., Luksepp, T., and Osnes, H. Low-velocity impact response of injection-moulded polypropylene plates – Part 2: Effects of moulding conditions, striker geometry, clamping, surface texture, weld line and paint. *Polymer Testing*, 2010; 29(7): p. 894-901.
- [26] Liu, Y. and Liaw, B. Effects of constituents and lay-up configuration on drop-weight tests of fiber-metal laminates. *Applied Composite Materials*, 2010; 17(1): p. 43-62.
- [27] Abdullah, M.R. and Cantwell, W.J. The impact resistance of polypropylene-based fibre–metal laminates. *Composites Science and Technology*, 2006; 66(11–12): p. 1682-1693.
- [28] Cortés, P. and Cantwell, W.J. The fracture properties of a fibre–metal laminate based on magnesium alloy. *Composites Part B: Engineering*, 2005; 37(2–3): p. 163-170.
- [29] Alderliesten, R., Rans, C., and Benedictus, R. The applicability of magnesium based Fibre Metal Laminates in aerospace structures. *Composites Science and Technology*, 2008; 68(14): p. 2983-2993.
- [30] Sadighi, M., Pärnänen, T., Alderliesten, R.C., Sayeafabi, M., and Benedictus, R. Experimental and numerical investigation of metal type and thickness effects on the impact resistance of fiber metal laminates. *Applied Composite Materials*, 2012; 19(3-4): p. 545-559.
- [31] Chen, Y., Chen, L., Huang, Q., and Zhang, Z. Effect of metal type on the energy absorption of fiber metal laminates under low-velocity impact. *Mechanics of Advanced Materials and Structures*, 2021: p. 1-17.

- [32] Burianek, D.A. and Spearing, S.M. Fatigue damage in titanium-graphite hybrid laminates. *Composites Science and Technology*, 2002; 62(5): p. 607-617.
- [33] Jakubczak, P., Bieniaś, J., and Drożdziel, M. The collation of impact behaviour of titanium/carbon, aluminum/carbon and conventional carbon fibres laminates. *Thin-Walled Structures*, 2020; 155: p. 106952.
- [34] Jaroslaw, B., Barbara, S., and Patryk, J. The comparison of low-velocity impact resistance of aluminum/carbon and glass fiber metal laminates. *Polymer Composites*, 2016; 37(4): p. 1056-1063.
- [35] Sisan, M.M. and Eslami-Farsani, R. An experimental study on impact resistance of different layup configuration of fiber metal laminates. *Fibers and Polymers*, 2019; 20(10): p. 2200-2206.
- [36] Ferrante, L., Sarasini, F., Tirillò, J., Lampani, L., Valente, T., and Gaudenzi, P. Low velocity impact response of basalt-aluminium fibre metal laminates. *Materials & Design*, 2016; 98: p. 98-107.
- [37] Li, X., Zhang, X., Guo, Y., Shim, V.P.W., Yang, J., and Chai, G.B. Influence of fiber type on the impact response of titanium-based fiber-metal laminates. *International Journal of Impact Engineering*, 2018; 114: p. 32-42.
- [38] Hussain, M., Imad, A., Saouab, A., Nawab, Y., Kanit, T., Herbelot, C., and Muhammad, K. Properties and characterization of novel 3D jute reinforced natural fibre aluminium laminates. *Journal of Composite Materials*, 2020; 55.
- [39] Subramaniam, K., Dhar Malingam, S., Feng, N.L., and Bapokutty, O. The effects of stacking configuration on the response of tensile and quasi-static penetration to woven kenaf/glass hybrid composite metal laminate. *Polymer Composites*, 2019; 40(2): p. 568-577.
- [40] Feng, N.L., Malingam, S.D., and Ping, C.W. Mechanical characterisation of kenaf/PALF reinforced composite-metal laminates: Effects of hybridisation and weaving architectures. *Journal of Reinforced Plastics and Composites*; 40(5-6): p. 193-205.
- [41] Badawy, A.A.M. Impact behavior of glass fibers reinforced composite laminates at different temperatures. *Ain Shams Engineering Journal*, 2012; 3(2): p. 105-111.
- [42] Ibekwe, S.I., Mensah, P.F., Li, G., Pang, S.-S., and Stubblefield, M.A. Impact and post impact response of laminated beams at low temperatures. *Composite Structures*, 2007; 79(1): p. 12-17.
- [43] Zhu, S. and Chai, G.B. Low-velocity impact response of fibre–metal laminates – Experimental and finite element analysis. *Composites Science and Technology*, 2012; 72(15): p. 1793-1802.
- [44] Seyed Yaghoubi, A. and Liaw, B. Thickness influence on ballistic impact behaviors of GLARE 5 fiber-metal laminated beams: Experimental and numerical studies. *Composite Structures*, 2012; 94(8): p. 2585-2598.
- [45] Seyed Yaghoubi, A. and Liaw, B. Effect of lay-up orientation on ballistic impact behaviors of GLARE 5 FML beams. *International Journal of Impact Engineering*, 2013; 54: p. 138-148.
- [46] Hagi Kashani, M., Sadighi, M., Mohammadkhah, M., and Shahsavari Alavijeh, H. Investigation of scaling effects on fiber metal laminates under tensile and flexural loading. *Proceedings of the Institution of Mechanical Engineers, Part L: Journal of Materials Design and Applications*, 2013; 229(3): p. 189-201.
- [47] Song, S.H., Byun, Y.S., Ku, T.W., Song, W.J., Kim, J., and Kang, B.S. Experimental and numerical investigation on impact performance of carbon

- reinforced aluminum laminates. *Journal of Materials Science & Technology*, 2010; 26(4): p. 327-332.
- [48] Tsartsaris, N., Meo, M., Dolce, F., Polimeno, U., Guida, M., and Marulo, F. Low-velocity impact behavior of fiber metal laminates. *Journal of Composite Materials*, 2011; 45(7): p. 803-814.
- [49] Jakubczak, P., Bienias, J., and Surowska, B. The influence of fibre orientation in aluminium–carbon laminates on low-velocity impact resistance. *Journal of Composite Materials*, 2017; 52(8): p. 1005-1016.
- [50] Asaee, Z., Shadlou, S., and Taheri, F. Low-velocity impact response of fiberglass/magnesium FMLs with a new 3D fiberglass fabric. *Composite Structures*, 2015; 122: p. 155-165.
- [51] Asaee, Z. and Taheri, F. Enhancement of performance of three-dimensional fiber metal laminates under low velocity impact – A coupled numerical and experimental investigation. *Journal of Sandwich Structures & Materials*, 2019; 21(6): p. 2127-2153.
- [52] De Cicco, D. and Taheri, F. Performances of magnesium- and steel-based 3D fiber-metal laminates under various loading conditions. *Composite Structures*, 2019; 229: p. 111390.
- [53] Shanmugam, L., Kazemi, M., Qiu, C., Rui, M., Yang, L., and Yang, J. Influence of UHMWPE fiber and Ti6Al4V metal surface treatments on the low-velocity impact behavior of thermoplastic fiber metal laminates. *Advanced Composites and Hybrid Materials*, 2020; 3: p. 508 - 521.
- [54] Hu, Y., Li, H., Tao, J., Pan, L., and Xu, J. The effects of temperature variation on mechanical behaviors of polyetheretherketone - based fiber metal laminates. *Polymer Composites*, 2016.
- [55] Reyes V, G. and Cantwell, W.J. The mechanical properties of fibre-metal laminates based on glass fibre reinforced polypropylene. *Composites Science and Technology*, 2000; 60(7): p. 1085-1094.
- [56] Santiago, R., Cantwell, W., and Alves, M. Impact on thermoplastic fibre-metal laminates: Experimental observations. *Composite Structures*, 2017; 159: p. 800-817.
- [57] Fan, J., Guan, Z.W., and Cantwell, W.J. Numerical modelling of perforation failure in fibre metal laminates subjected to low velocity impact loading. *Composite Structures*, 2011; 93(9): p. 2430-2436.
- [58] Sharma, A.P., Khan, S.H., Kitey, R., and Parameswaran, V. Effect of through thickness metal layer distribution on the low velocity impact response of fiber metal laminates. *Polymer Testing*, 2018; 65: p. 301-312.
- [59] Droździel, M., Jakubczak, P., and Bieniaś, J. Low-velocity impact resistance of thin-ply in comparison with conventional aluminium-carbon laminates. *Composite Structures*, 2021; 256: p. 113083.
- [60] Meng, X., Yao, L., Wang, C., He, W., Xie, L., and Zhang, H. Investigation on the low-velocity impact behaviour of non-symmetric FMLs—experimental and numerical methods. *International Journal of Crashworthiness*, 2020: p. 1-19.
- [61] Wu, H.F., Wu, L.L., Slagter, W.J., and Verolme, J.L. Use of rule of mixtures and metal volume fraction for mechanical property predictions of fibre-reinforced aluminium laminates. *Journal of Materials Science*, 1994; 29: p. 4583-4591.

- [62] Patryk, J., Jaroslaw, B., Krzysztof, M., Monika, O., and Barbara, S. The impact behavior of aluminum hybrid laminates. *Aircraft Engineering and Aerospace Technology*, 2014; 86(4): p. 287-294.
- [63] Thomason, J.L. The influence of fibre length, diameter and concentration on the impact performance of long glass-fibre reinforced polyamide 6,6. *Composites Part A: Applied Science and Manufacturing*, 2009; 40(2): p. 114-124.
- [64] Vlot, A. and Van Ingen, J.W. Delamination resistance of post-stretched fibre metal laminates. *Journal of Composite Materials*, 1998; 32(19): p. 1784-1805.
- [65] Banea, M.D., Rosioara, M., Carbas, R.J.C., and da Silva, L.F.M. Multi-material adhesive joints for automotive industry. *Composites Part B: Engineering*, 2018; 151: p. 71-77.
- [66] Pärnänen, T., Vääntinen, A., Kanerva, M., Jokinen, J., and Saarela, O. The effects of debonding on the low-velocity impact response of steel-cfrp fibre metal laminates. *Applied Composite Materials*, 2016; 23(6): p. 1151-1166.
- [67] Gonzalez-Canche, N.G., Flores-Johnson, E.A., and Carrillo, J.G. Mechanical characterization of fiber metal laminate based on aramid fiber reinforced polypropylene. *Composite Structures*, 2017; 172: p. 259-266.
- [68] Hirai, Y., Hamada, H., and Kim, J.-K. Impact response of woven glass-fabric composites—I: Effect of fibre surface treatment. *Composites Science and Technology*, 1998; 58(1): p. 91-104.
- [69] Özşahin, E. and Tolun, S. Influence of surface coating on ballistic performance of aluminum plates subjected to high velocity impact loads. *Materials & Design*, 2010; 31(3): p. 1276-1283.
- [70] Hu, Y.B., Li, H.G., Cai, L., Zhu, J.P., Pan, L., Xu, J., and Tao, J. Preparation and properties of Fibre–Metal Laminates based on carbon fibre reinforced PMR polyimide. *Composites Part B: Engineering*, 2015; 69: p. 587-591.
- [71] Abdullah, M.R., Prawoto, Y., and Cantwell, W.J. Interfacial fracture of the fibre-metal laminates based on fibre reinforced thermoplastics. *Materials & Design*, 2015; 66, Part B: p. 446-452.
- [72] Yu, G.-C., Wu, L.-Z., Ma, L., and Xiong, J. Low velocity impact of carbon fiber aluminum laminates. *Composite Structures*, 2015; 119: p. 757-766.
- [73] Khan, S.H., Sharma, A.P., Kitey, R., and Parameswaran, V. Effect of metal layer placement on the damage and energy absorption mechanisms in aluminium/glass fibre laminates. *International Journal of Impact Engineering*, 2018; 119: p. 14-25.
- [74] De Cicco, D., Asaee, Z., and Taheri, F. Low-velocity impact damage response of fiberglass/magnesium fiber-metal laminates under different size and shape impactors. *Mechanics of Advanced Materials and Structures*, 2017; 24(7): p. 545-555.
- [75] Ortiz de Mendibil, I., Aretxabaleta, L., Sarrionandia, M., Mateos, M., and Aurrekoetxea, J. Impact behaviour of glass fibre-reinforced epoxy/aluminium fibre metal laminate manufactured by Vacuum Assisted Resin Transfer Moulding. *Composite Structures*, 2016; 140: p. 118-124.
- [76] Mamalis, D., Obande, W., Koutsos, V., Blackford, J.R., Ó Brádaigh, C.M., and Ray, D. Novel thermoplastic fibre-metal laminates manufactured by vacuum resin infusion: The effect of surface treatments on interfacial bonding. *Materials & Design*, 2019; 162: p. 331-344.

- [77] Caprino, G., Spataro, G., and Del Luongo, S. Low-velocity impact behaviour of fibreglass–aluminium laminates. *Composites Part A: Applied Science and Manufacturing*, 2004; 35(5): p. 605-616.
- [78] Khalid, A.A. The effect of testing temperature and volume fraction on impact energy of composites. *Materials & Design*, 2006; 27(6): p. 499-506.
- [79] Low, K.O., Teng, S.M., Johar, M., Israr, H.A., and Wong, K.J. Mode I delamination behaviour of carbon/epoxy composite at different displacement rates. *Composites Part B: Engineering*, 2019; 176: p. 107293.
- [80] Jakubczak, P. and Bieniaś, J. Comparison of quasi static indentation and dynamic loads of glass and carbon fibre aluminium laminates. Vol. 88. 2016. 404-410.
- [81] Nassir, N.A., Birch, R.S., Cantwell, W.J., Sierra, D.R., Edwardson, S.P., Dearden, G., and Guan, Z.W. Experimental and numerical characterization of titanium-based fibre metal laminates. *Composite Structures*, 2020; 245: p. 112398.
- [82] Taghizadeh, S.A., Liaghat, G., Niknejad, A., and Pedram, E. Experimental study on quasi-static penetration process of cylindrical indenters with different nose shapes into the hybrid composite panels. *Journal of Composite Materials*, 2019; 53(1): p. 107-123.
- [83] Hagi Kashani, M., Sadighi, M., Lalehpour, A., and Alderliesten, R. The effect of impact energy division over repeated low-velocity impact on fiber metal laminates. *Journal of Composite Materials*, 2014.
- [84] Richardson, M.O.W. and Wisheart, M.J. Review of low-velocity impact properties of composite materials. *Composites Part A: Applied Science and Manufacturing*, 1996; 27(12): p. 1123-1131.
- [85] Tsamasphyros, G.J. and Bikakis, G.S. Analytical modeling to predict the low velocity impact response of circular GLARE fiber–metal laminates. *Aerospace Science and Technology*, 2013; 29(1): p. 28-36.
- [86] Bibo, G., Leicy, D., Hogg, P.J., and Kemp, M. High-temperature damage tolerance of carbon fibre-reinforced plastics. *Composites*, 1994; 25(6): p. 414-424.
- [87] Jakubczak, P., Bieniaś, J., and Dadej, K. Experimental and numerical investigation into the impact resistance of aluminium carbon laminates. *Composite Structures*, 2020; 244: p. 112319.
- [88] Ahmadi, H., Ekrami, M., Sabouri, H., and Bayat, M. Experimental and numerical investigation on the effect of projectile nose shape in low-velocity impact loading on fiber metal laminate panels. *Proceedings of the Institution of Mechanical Engineers, Part G: Journal of Aerospace Engineering*, 2019; 233(10): p. 3665-3679.
- [89] Li, L., Sun, L., Wang, T., Kang, N., and Cao, W. Repeated low-velocity impact response and damage mechanism of glass fiber aluminium laminates. *Aerospace Science and Technology*, 2019; 84: p. 995-1010.
- [90] Heydari-Meybodi, M., Mohammadkhani, H., and Bagheri, M. Oblique low-velocity impact on fiber-metal laminates. *Applied Composite Materials*, 2017; 24.
- [91] Yao, L., Sun, G., He, W., Meng, X., and Xie, D. Investigation on impact behavior of FMLs under multiple impacts with the same total energy: Experimental characterization and numerical simulation. *Composite Structures*, 2019; 226: p. 111218.

- [92] Morinière, F.D., Alderliesten, R.C., and Benedictus, R. Modelling of impact damage and dynamics in fibre-metal laminates – A review. *International Journal of Impact Engineering*, 2014; 67: p. 27-38.
- [93] Hirai, Y., Hamada, H., and Kim, J.-K. Impact response of woven glass-fabric composites—II. Effect of temperature. *Composites Science and Technology*, 1998; 58(1): p. 119-128.
- [94] Hoo Fatt, M.S., Lin, C., Revilock Jr, D.M., and Hopkins, D.A. Ballistic impact of GLARE™ fiber–metal laminates. *Composite Structures*, 2003; 61(1–2): p. 73-88.
- [95] Daniel, I.M., Werner, B.T., and Fenner, J.S. Strain-rate-dependent failure criteria for composites. *Composites Science and Technology*, 2011; 71(3): p. 357-364.
- [96] Shokrieh, M.M. and Omid, M.J. Investigating the transverse behavior of Glass–Epoxy composites under intermediate strain rates. *Composite Structures*, 2011; 93(2): p. 690-696.
- [97] Alderliesten, R.C. On the available relevant approaches for fatigue crack propagation prediction in Glare. *International Journal of Fatigue*, 2007; 29(2): p. 289-304.
- [98] Alderliesten, R.C. Analytical prediction model for fatigue crack propagation and delamination growth in Glare. *International Journal of Fatigue*, 2007; 29(4): p. 628-646.
- [99] Guo, Y.-J. and Wu, X.-R. A phenomenological model for predicting crack growth in fiber-reinforced metal laminates under constant-amplitude loading. *Composites Science and Technology*, 1999; 59(12): p. 1825-1831.
- [100] Hashemi, S., Kinloch, A.J., and Williams, J.G. The effects of geometry, rate and temperature on the Mode I, Mode II and Mixed-Mode I/II interlaminar fracture of carbon-fibre/poly(ether-ether ketone) composites. *Journal of Composite Materials*, 1990; 24(9): p. 918-956.
- [101] Johar, M., Wong, K.J., and Tamin, N. Mixed-Mode delamination failures of quasi-isotropic quasi-homogeneous carbon/epoxy laminated composite. 2017.
- [102] Reis, P.N.B., Ferreira, J.A.M., Antunes, F.V., and Costa, J.D.M. Initial crack length on the interlaminar fracture of woven carbon/epoxy laminates. *Fibers and Polymers*, 2015; 16(4): p. 894-901.
- [103] Carrillo, J.G. and Cantwell, W.J. Mechanical properties of a novel fiber–metal laminate based on a polypropylene composite. *Mechanics of Materials*, 2009; 41(7): p. 828-838.
- [104] Hasan, M.Z. Interface failure of heated GLARE™ Fiber–Metal Laminates under bird strike. *Aerospace*, 2020; 7(3): p. 28.
- [105] Zarei, H., Fallah, M., Minak, G., Bisadi, H., and Daneshmehr, A. Low velocity impact analysis of Fiber Metal Laminates (FMLs) in thermal environments with various boundary conditions. *Composite Structures*, 2016; 149: p. 170-183.
- [106] Huda, Z., Zaharinie, T., and Min, G.J. Temperature effects on material behavior of aerospace aluminum alloys for subsonic and supersonic aircraft. *Journal of Aerospace Engineering*, 2010; 23(2).
- [107] Dimitrienko, Y.I. Thermomechanical behaviour of composite materials and structures under high temperatures: 2. Structures. *Composites Part A: Applied Science and Manufacturing*, 1997; 28(5): p. 463-471.

- [108] Zhang, L., Liu, W., Sun, G., Wang, L., and Li, L.-z. Two-dimensional modeling of thermomechanical responses of rectangular GFRP profiles exposed to fire. Vol. 2017. 2017. 1-17.
- [109] Rans, C.D., Alderliesten, R.C., and Benedictus, R. Predicting the influence of temperature on fatigue crack propagation in Fibre Metal Laminates. *Engineering Fracture Mechanics*, 2011; 78(10): p. 2193-2201.
- [110] Seidt, J.D. and Gilat, A. Plastic deformation of 2024-T351 aluminum plate over a wide range of loading conditions. *International Journal of Solids and Structures*, 2013; 50(10): p. 1781-1790.
- [111] Bai, Y. and Keller, T. Modeling of mechanical response of FRP composites in fire. *Composites Part A: Applied Science and Manufacturing*, 2009; 40(6): p. 731-738.
- [112] Bai, Y., Keller, T., and Vallée, T. Modeling of stiffness of FRP composites under elevated and high temperatures. *Composites Science and Technology*, 2008; 68(15): p. 3099-3106.
- [113] Ou, Y. and Zhu, D. Tensile behavior of glass fiber reinforced composite at different strain rates and temperatures. *Construction and Building Materials*, 2015; 96: p. 648-656.
- [114] Kumar, M.K., Krishna, D., and Chandra, R.B. High - temperature tensile behavior at different crosshead speeds during loading of glass fiber - reinforced polymer composites. *Journal of Applied Polymer Science*, 2017; 134(16).
- [115] Gabrion, X., Placet, V., Trivaudey, F., and Boubakar, L. About the thermomechanical behaviour of a carbon fibre reinforced high-temperature thermoplastic composite. *Composites Part B: Engineering*, 2016; 95: p. 386-394.
- [116] Hawileh, R.A., Abu-Obeidah, A., Abdalla, J.A., and Al-Tamimi, A. Temperature effect on the mechanical properties of carbon, glass and carbon-glass FRP laminates. *Construction and Building Materials*, 2015; 75: p. 342-348.
- [117] Jarrah, M., Najafabadi, E.P., Khaneghahi, M.H., and Oskouei, A.V. The effect of elevated temperatures on the tensile performance of GFRP and CFRP sheets. *Construction and Building Materials*, 2018; 190: p. 38-52.
- [118] Lu, Z., Xian, G., and Li, H. Effects of elevated temperatures on the mechanical properties of basalt fibers and BFRP plates. *Construction and Building Materials*, 2016; 127: p. 1029-1036.
- [119] Rosa, I., Morgado, T., Correia, J., Firmo, J., and Silvestre, N. Shear behavior of GFRP composite materials at elevated temperature. Vol. 22. 2018. 04018010.
- [120] Wang, L., Fan, X., Chen, H., and Liu, W. Axial crush behavior and energy absorption capability of foam-filled GFRP tubes under elevated and high temperatures. *Composite Structures*, 2016; 149: p. 339-350.
- [121] Aklilu, G., Adali, S., and Bright, G. Temperature effect on mechanical properties of carbon, glass and hybrid polymer composite specimens. Vol. 39. 2018. 119-138.
- [122] Bazli, M., Ashrafi, H., Jafari, A., Zhao, X.-L., Gholipour, H., and Oskouei, A.V. Effect of thickness and reinforcement configuration on flexural and impact behaviour of GFRP laminates after exposure to elevated temperatures. *Composites Part B: Engineering*, 2019; 157: p. 76-99.

- [123] Houshmand, M., Jarrah, M., and Pournamazian Najafabadi, E. The effect of elevated temperatures on the tensile performance of GFRP and CFRP sheets. Vol. 190. 2018. 38-52.
- [124] Gibson, A.G., Wu, Y.S., Evans, J.T., and Mouritz, A.P. Laminate theory analysis of composites under load in fire. *Journal of Composite Materials*, 2005; 40(7): p. 639-658.
- [125] Mahieux, C.A., Reifsnider, K.L., and Case, S.W. Property modeling across transition temperatures in PMC's: Part i. Tensile properties. *Applied Composite Materials*, 2001; 8(4): p. 217-234.
- [126] Sengodan, G.A., Allegri, G., and Hallett, S.R. Simulation of progressive failure in laminated composites under variable environmental conditions. *Materials & Design*, 2020; 196: p. 109082.
- [127] Ramírez, F.M.G., Garpelli, F.P., Sales, R.d.C.M., Cândido, G.M., Arbelo, M.A., Shiino, M.Y., and Donadon, M.V. Hygrothermal effects on the fatigue delamination growth onset in interlayer toughened CFRP joints. *International Journal of Fatigue*, 2020; 138: p. 105729.
- [128] Tsokanas, P. and Loutas, T. Hygrothermal effect on the strain energy release rates and mode mixity of asymmetric delaminations in generally layered beams. *Engineering Fracture Mechanics*, 2019; 214: p. 390-409.
- [129] Tsokanas, P., Loutas, T., Kotsinis, G., Kostopoulos, V., van den Brink, W.M., and Martin de la Escalera, F. On the fracture toughness of metal-composite adhesive joints with bending-extension coupling and residual thermal stresses effect. *Composites Part B: Engineering*, 2020; 185: p. 107694.
- [130] Czabaj, M.W. and Davidson, B.D. Determination of the mode I, mode II, and mixed-mode I–II delamination toughness of a graphite/polyimide composite at room and elevated temperatures. *Journal of Composite Materials*, 2015; 50(16): p. 2235-2253.
- [131] Charalambous, G., Allegri, G., and Hallett, S.R. Temperature effects on mixed mode I/II delamination under quasi-static and fatigue loading of a carbon/epoxy composite. *Composites Part A: Applied Science and Manufacturing*, 2015; 77: p. 75-86.
- [132] Argüelles, A., Viña, J., Canteli, A.F., Coronado, P., and Mollón, V. Influence of temperature on the delamination process under mode I fracture and dynamic loading of two carbon–epoxy composites. *Composites Part B: Engineering*, 2015; 68: p. 207-214.
- [133] Cadieu, L., Kopp, J.B., Jumel, J., Bega, J., and Froustey, C. A fracture behaviour evaluation of Glass/Elium150 thermoplastic laminate with the DCB test: Influence of loading rate and temperature. *Composite Structures*, 2021; 255: p. 112907.
- [134] Davidson, B.D., Kumar, M., and Soffa, M.A. Influence of mode ratio and hygrothermal condition on the delamination toughness of a thermoplastic particulate interlayered carbon/epoxy composite. *Composites Part A: Applied Science and Manufacturing*, 2009; 40(1): p. 67-79.
- [135] Wu, H.F. Effect of temperature and strain rate on tensile mechanical properties of ARALL-1 laminates. *Journal of Materials Science*, 1991; 26(14): p. 3721-3729.
- [136] Wu, H.F. Temperature dependence of the tensile behaviour of aramid/aluminium laminates. *Journal of Materials Science*, 1993; 28(1): p. 19-34.

- [137] Sarasini, F., Tirillò, J., Ferrante, L., Sergi, C., Sbardella, F., Russo, P., Simeoli, G., Mellier, D., and Calzolari, A. Effect of temperature and fiber type on impact behavior of thermoplastic fiber metal laminates. *Composite Structures*, 2019; 223: p. 110961.
- [138] Cortés, P. and Cantwell, W.J. The impact properties of high-temperature fiber-metal laminates. *Journal of Composite Materials*, 2006; 41(5): p. 613-632.
- [139] da Costa, A.A., da Silva, D., Travessa, D.N., and Botelho, E.C. The effect of thermal cycles on the mechanical properties of fiber-metal laminates. *Materials & Design*, 2012; 42: p. 434-440.
- [140] Li, H., Hu, Y., Liu, C., Zheng, X., Liu, H., and Tao, J. The effect of thermal fatigue on the mechanical properties of the novel fiber metal laminates based on aluminum–lithium alloy. *Composites Part A: Applied Science and Manufacturing*, 2016; 84: p. 36-42.
- [141] Müller, B., Hagenbeek, M., and Sinke, J. Thermal cycling of (heated) fibre metal laminates. *Composite Structures*, 2016; 152: p. 106-116.
- [142] López-Puente, J., Zaera, R., and Navarro, C. The effect of low temperatures on the intermediate and high velocity impact response of CFRPs. *Composites Part B: Engineering*, 2002; 33(8): p. 559-566.
- [143] Morinière, F.D., Alderliesten, R.C., and Benedictus, R. Low-velocity impact energy partition in GLARE. *Mechanics of Materials*, 2013; 66: p. 59-68.
- [144] Yao, L., Wang, C., He, W., Lu, S., and Xie, D. Influence of impactor shape on low-velocity impact behavior of fiber metal laminates combined numerical and experimental approaches. *Thin-Walled Structures*, 2019; 145: p. 106399.
- [145] Cantwell, W.J. and Morton, J. Impact perforation of carbon fibre reinforced plastic. *Composites Science and Technology*, 1990; 38(2): p. 119-141.
- [146] Seo, H., Hundley, J., Hahn, H.T., and Yang, J.-M. Numerical simulation of glass-fiber-reinforced aluminum laminates with diverse impact damage. *AIAA Journal*, 2010; 48(3): p. 676-687.
- [147] Iannucci, L. Progressive failure modelling of woven carbon composite under impact. *International Journal of Impact Engineering*, 2006; 32(6): p. 1013-1043.
- [148] Azhdari, S., Fakhreddini-Najafabadi, S., and Taheri-Behrooz, F. An experimental and numerical investigation on low velocity impact response of GLAREs. *Composite Structures*, 2021; 271: p. 114123.
- [149] Wang, P., Yang, J., Liu, M., Zhang, X., Sun, D., Bao, C., Gao, G., Yahya, Y., and Songlin, x. Modification of the contact surfaces for improving the puncture resistance of laminar structures. *Scientific Reports*, 2017; 7.
- [150] Payeganeh, G.H., Ashenai Ghasemi, F., and Malekzadeh, K. Dynamic response of fiber–metal laminates (FMLs) subjected to low-velocity impact. *Thin-Walled Structures*, 2010; 48(1): p. 62-70.
- [151] Abrate, S. Modeling of impacts on composite structures. *Composite Structures*, 2001; 51(2): p. 129-138.
- [152] Langdon, G.S., Lemanski, S.L., Nurick, G.N., Simmons, M.C., Cantwell, W.J., and Schleyer, G.K. Behaviour of fibre–metal laminates subjected to localised blast loading: Part I—Experimental observations. *International Journal of Impact Engineering*, 2007; 34(7): p. 1202-1222.
- [153] Lemanski, S.L., Nurick, G.N., Langdon, G.S., Simmons, M.C., Cantwell, W.J., and Schleyer, G.K. Behaviour of fibre metal laminates subjected to localised blast loading—Part II: Quantitative analysis. *International Journal of Impact Engineering*, 2007; 34(7): p. 1223-1245.

- [154] Morinière, F.D., Alderliesten, R.C., Sadighi, M., and Benedictus, R. An integrated study on the low-velocity impact response of the GLARE fibre-metal laminate. *Composite Structures*, 2013; 100: p. 89-103.
- [155] Ibrahim, G.R. and Albarbar, A. A new approach to the cohesive zone model that includes thermal effects. *Composites Part B: Engineering*, 2019; 167: p. 370-376.
- [156] Günther, N., Griese, M., Stammen, E., and Dilger, K. Modeling of adhesive layers with temperature-dependent cohesive zone elements for predicting adhesive failure during the drying process of cathodic dip painting. *Proceedings of the Institution of Mechanical Engineers, Part L: Journal of Materials: Design and Applications*, 2019; 233(3): p. 485-494.
- [157] Bikakis, G.S.E. and Savaidis, A. FEM simulation of simply supported GLARE plates under lateral indentation loading and unloading. *Theoretical and Applied Fracture Mechanics*, 2016; 83: p. 2-10.
- [158] Bikakis, G.S. Response of circular GLARE fiber–metal laminates subjected to oblique indentation. *Journal of Reinforced Plastics and Composites*, 2016; 35(18): p. 1329-1341.
- [159] Bikakis, G.S. Finite element and analytical modeling to predict the frictional oblique indentation response of GLARE fiber–metal laminates. *Journal of Reinforced Plastics and Composites*, 2017; 36(11): p. 797-807.
- [160] Bienias, J., Jakubczak, P., and Dadej, K. Low-velocity impact resistance of aluminium glass laminates – Experimental and numerical investigation. *Composite Structures*, 2016; 152: p. 339-348.
- [161] Frizzell, R.M., McCarthy, C.T., and McCarthy, M.A. Simulating damage and delamination in fibre metal laminate joints using a three-dimensional damage model with cohesive elements and damage regularisation. *Composites Science and Technology*, 2011; 71(9): p. 1225-1235.
- [162] Karagiozova, D., Langdon, G.S., Nurick, G.N., and Chung Kim Yuen, S. Simulation of the response of fibre–metal laminates to localised blast loading. *International Journal of Impact Engineering*, 2010; 37(6): p. 766-782.
- [163] Hashagen, F. and de Borst, R. Numerical assessment of delamination in fibre metal laminates. *Computer Methods in Applied Mechanics and Engineering*, 2000; 185(2–4): p. 141-159.
- [164] Johnson, G.R. and Cook, W.H. Fracture characteristics of three metals subjected to various strains, strain rates, temperatures and pressures. *Engineering Fracture Mechanics*, 1985; 21(1): p. 31-48.
- [165] Matzenmiller, A., Lubliner, J., and Taylor, R.L. A constitutive model for anisotropic damage in fiber-composites. *Mechanics of Materials*, 1995; 20(2): p. 125-152.
- [166] Barbieri, E. and Meo, M. A meshfree penalty-based approach to delamination in composites. *Composites Science and Technology*, 2009; 69(13): p. 2169-2177.
- [167] Pascoe, J.A., Alderliesten, R.C., and Benedictus, R. Methods for the prediction of fatigue delamination growth in composites and adhesive bonds – A critical review. *Engineering Fracture Mechanics*, 2013; 112–113: p. 72-96.
- [168] Turon, A., Dávila, C.G., Camanho, P.P., and Costa, J. An engineering solution for mesh size effects in the simulation of delamination using cohesive zone models. *Engineering Fracture Mechanics*, 2007; 74(10): p. 1665-1682.
- [169] Turon, A., Camanho, P.P., Costa, J., and Renart, J. Accurate simulation of delamination growth under mixed-mode loading using cohesive elements:

- Definition of interlaminar strengths and elastic stiffness. *Composite Structures*, 2010; 92(8): p. 1857-1864.
- [170] LeBlanc, L.R. and LaPlante, G. Experimental investigation and finite element modeling of mixed-mode delamination in a moisture-exposed carbon/epoxy composite. *Composites Part A: Applied Science and Manufacturing*, 2016; 81: p. 202-213.
- [171] Johar, M., Israr, H.A., Low, K.O., and Wong, K.J. Numerical simulation methodology for mode II delamination of quasi-isotropic quasi-homogeneous composite laminates. *Journal of Composite Materials*, 2017; 51(28): p. 3955-3968.
- [172] R. Kolor, S.S. and Tamin, M.N. Mode-II interlaminar fracture and crack-jump phenomenon in CFRP composite laminate materials. *Composite Structures*, 2018; 204: p. 594-606.
- [173] Liao, B.B. and Liu, P.F. Finite element analysis of dynamic progressive failure properties of GLARE hybrid laminates under low-velocity impact. *Journal of Composite Materials*, 2017; 52(10): p. 1317-1330.
- [174] Li, H., Xu, Y., Hua, X., Liu, C., and Tao, J. Bending failure mechanism and flexural properties of GLARE laminates with different stacking sequences. *Composite Structures*, 2018; 187: p. 354-363.
- [175] Manikandan, P. and Chai, G.B. Mode-I metal-composite interface fracture testing for fibre metal laminates. *Advances in Materials Science and Engineering*, 2018; 2018: p. 11.
- [176] Zhao, L., Gong, Y., Zhang, J., Chen, Y., and Fei, B. Simulation of delamination growth in multidirectional laminates under mode I and mixed mode I/II loadings using cohesive elements. *Composite Structures*, 2014; 116: p. 509-522.
- [177] Delbariani-Nejad, A., Malakouti, M., and Farrokhhabadi, A. Reliability analysis of metal - composite adhesive joints under debonding modes I, II, and I/II using the results of experimental and FEM analyses. *Fatigue & Fracture of Engineering Materials & Structures*, 2019; 42: p. 2644-2662.
- [178] Qin, G., Na, J., Tan, W., Mu, W., and Ji, J. Failure prediction of adhesively bonded CFRP-Aluminum alloy joints using cohesive zone model with consideration of temperature effect. *The Journal of Adhesion*, 2019; 95(8): p. 723-746.
- [179] Sun, X.C. and Hallett, S.R. Barely visible impact damage in scaled composite laminates: Experiments and numerical simulations. *International Journal of Impact Engineering*, 2017; 109: p. 178-195.
- [180] Shi, Y., Pinna, C., and Soutis, C. Impact damage characteristics of carbon fibre metal laminates: Experiments and simulation. *Applied Composite Materials*, 2020; 27(5): p. 511-531.
- [181] Shi, Y., Pinna, C., and Soutis, C. Modelling impact damage in composite laminates: A simulation of intra- and inter-laminar cracking. *Composite Structures*, 2014; 114: p. 10-19.
- [182] Lesuer, D. Experimental investigations of material models for TI-6Al-4V titanium and 2024-t3 aluminum. 2000, Lawrence Livermore National Lab.: United States.
- [183] ASTM D3039 / D3039M-14, Standard test method for tensile properties of polymer matrix composite materials. ASTM International, West Conshohocken, PA, 2014.

- [184] ASTM D6641 / D6641M-14, Standard test method for compressive properties of polymer matrix composite materials using a combined loading compression (CLC) test fixture. ASTM International, West Conshohocken, PA, 2014.
- [185] ASTM D3518 / D3518M-13, Standard test method for in-plane shear response of polymer matrix composite materials by tensile test of a $\pm 45^\circ$ laminate. ASTM International, West Conshohocken, PA, 2013.
- [186] ASTM D5528-13, Standard test method for mode I interlaminar fracture toughness of unidirectional fiber-reinforced polymer matrix composites. ASTM International, West Conshohocken, PA, 2013.
- [187] ASTM D7905 / D7905M-14, Standard test method for determination of the Mode II interlaminar fracture toughness of unidirectional fiber-reinforced polymer matrix composites. ASTM International, West Conshohocken, PA, 2014.
- [188] Chow, Z.P., Ahmad, Z., Wong, K.J., and Israr, H.A. Thermo-mechanical characterisation and modelling of GFRP laminated aluminium. *Composites Part B: Engineering*, 2019; 173: p. 106971.
- [189] Chang, F.-K. and Chang, K.-Y. A progressive damage model for laminated composites containing stress concentrations. *Journal of Composite Materials*, 1987; 21(9): p. 834-855.
- [190] Gerlach, S., Fiolka, M., and Matzenmiller, A. Modelling and analysis of adhesively bonded joints with interface elements for crash analysis. 2005.
- [191] Wong, K.J., Israr, H.A., and Tamin, M.N. Characterisation of moisture absorption effects on the strength of composite materials. *Advanced Materials Research*, 2015; 1125: p. 69-73.
- [192] Opelt, C., Faulstich de Paiva, J., Cândido, G.M., and Rezende, M.C. A fractographic study on the effects of hygrothermal conditioning on carbon fiber/epoxy laminates submitted to axial compression. Vol. 79. 2017.
- [193] Gong, Y., Zhao, L., Zhang, J., Wang, Y., and Hu, N. Delamination propagation criterion including the effect of fiber bridging for mixed-mode I/II delamination in CFRP multidirectional laminates. *Composites Science and Technology*, 2017; 151: p. 302-309.
- [194] Bosbach, B., Ohle, C., and Fiedler, B. Structural health monitoring of fibre metal laminates under mode I and II loading. *Composites Part A: Applied Science and Manufacturing*, 2018; 107: p. 471-478.
- [195] De Baere, I., Jacques, S., Van Paepegem, W., and Degrieck, J. Study of the Mode I and Mode II interlaminar behaviour of a carbon fabric reinforced thermoplastic. *Polymer Testing*, 2012; 31(2): p. 322-332.
- [196] Ou, Y., Zhu, D., Zhang, H., Huang, L., Yao, Y., Li, G., and Mobasher, B. Mechanical characterization of the tensile properties of glass fiber and its reinforced polymer (GFRP) composite under varying strain rates and temperatures. Vol. 8. 2016. 196.
- [197] Wong, K.J. Moisture absorption characteristics and effects on mechanical behaviour of carbon/epoxy composite : application to bonded patch repairs of composite structures. 2013, Université de Bourgogne.
- [198] Vlot, A.D., Kroon, E., and La Rocca, G. Impact response of fiber metal laminates. *Key Engineering Materials - KEY ENG MAT*, 1998; 141-143: p. 235-276.
- [199] Jakubczak, P. The impact behaviour of hybrid titanium glass laminates—Experimental and numerical approach. *International Journal of Mechanical Sciences*, 2019; 159: p. 58-73.

- [200] Wen, Q., li, W., Wang, W.B., Wang, F., Gao, Y.J., and Patel, V. Experimental and numerical investigations of bonding interface behavior in stationary shoulder friction stir lap welding. *Journal of Materials Science & Technology*, 2018; 35(1): p. 192-200.
- [201] Wong, K.J., Johar, M., Rahimian Kolor, S.S., Petru, M., and Tamin, M. Moisture absorption effects on Mode II delamination of carbon/epoxy composites. *Polymers*, 2020; 12: p. 1-13.
- [202] Pan, Y., Wu, G., Cheng, X., Zhang, Z., Li, M., Ji, S., and Huang, Z. Mode I and Mode II interlaminar fracture toughness of CFRP/magnesium alloys hybrid laminates. *Composite Interfaces*, 2016; 23(5): p. 453-465.
- [203] Yelamanchi, B., MacDonald, E., Gonzalez-Canche, N.G., Carrillo, J.G., and Cortes, P. The mechanical properties of fiber metal laminates based on 3D printed composites. *Materials*, 2020; 13(22): p. 5264.

LIST OF PUBLICATIONS

Journal with Impact Factor

1. **Chow, Z.P.**, Ahmad, Z., Wong, K.J., and Israr, H.A. Thermo-mechanical characterisation and modelling of GFRP laminated aluminium. *Composites Part B: Engineering*, 2019; 173: p. 106971.
<https://doi.org/10.1016/j.compositesb.2019.106971>. (Q1 ISI Indexed IF = **9.078**)
2. **Chow, Z.P.**, Ahmad, Z., Wong, K.J., Koloor, S.S.R., and Petru, M. Thermal Delamination Modelling and Evaluation of Aluminium-Glass Fibre-Reinforced Polymer Hybrid. *Polymers (Basel)*, 2021; 13(4): p. 492.
<https://doi.org/10.3390/polym13040492>. (Q1 ISI Indexed IF = **4.329**)
3. **Chow, Z.P.**, Ahmad, Z., Wong, K.J., and Syed Abdullah, S.I. Experimental and Numerical Analyses of Temperature Effect on Glare Panels under Quasi-Static Perforation. *Composite Structures*, 2021; 275: p. 114434.
<https://doi.org/10.1016/j.compstruct.2021.114434>. (Q2 ISI Indexed IF = **5.407**)
4. **Chow, Z.P.**, Ahmad, Z., and Wong, K.J. Temperature Effects on the Low-Velocity Impact of FML Panels: Experimental and Numerical Analyses. *International Journal of Impact Engineering [Under Review]*, 2021. (Q1 ISI Indexed IF = **4.208**)

Indexed Journal

1. **Chow, Z.P.**, Ahmad, Z., and Wong, K.J. Experimental Study on the Mechanical Properties of Glass Fiber Reinforced Epoxy at Elevated Temperature. *International Journal of Automotive and Mechanical Engineering*, 2019; 16(3): p. 7108-7120.

<https://doi.org/10.15282/ijame.16.3.2019.19.0531>. (Scopus Indexed SJR = 0.311)

Indexed Book Series

1. **Chow, Z.P.**, Ahmad, Z., and Wong, K.J. Experimental Study of Temperature Effect on the Mechanical Properties of GFRP and FML Interface. *Advanced Structured Materials*, 2020; 113: p. 47-58. https://doi.org/10.1007/978-3-030-20801-1_4. (Scopus Indexed SJR = 0.168)

Non-Indexed Journal

1. **Chow, Z.P.**, Ahmad, Z., and Wong, K.J. Temperature Effect Evaluation of FML Panels under Quasi Static Indentation Loading. *Science International (Lahore)*, 2019; 31(2): p. 291-295.

Indexed Conference Proceedings

1. Sofi, M., **Chow, Z.**, Wong, K.J., and Ahmad, Z. Study of multi-cell thin-walled tube with various configuration under lateral loading. *IOP Conference Series: Materials Science and Engineering*, 2020; 884: p. 012086. <https://doi.org/10.1088/1757-899X/884/1/012086>. (Scopus Indexed SJR = 0.198)